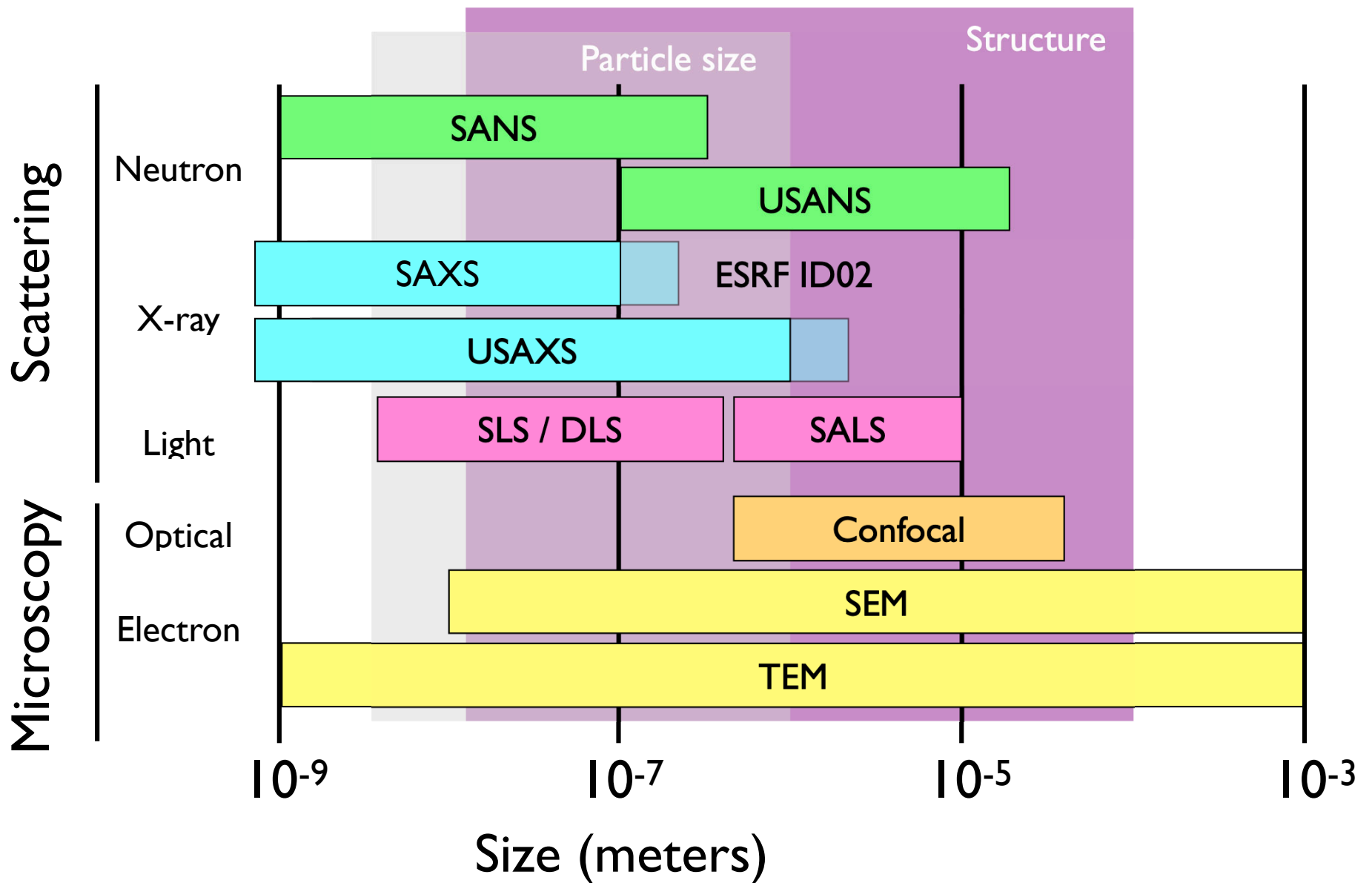# Methods of structural characterization
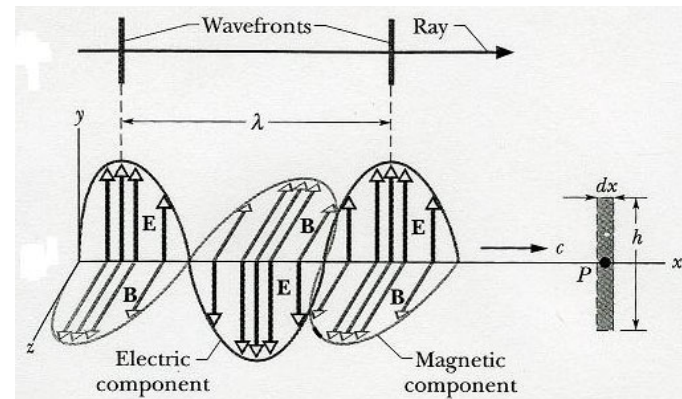
Structure characterization

Scattering

Scattering basics

Visible light and x-rays are transverse electromagnetic waves with perpendicular electric (E) and magnetic (B) components.
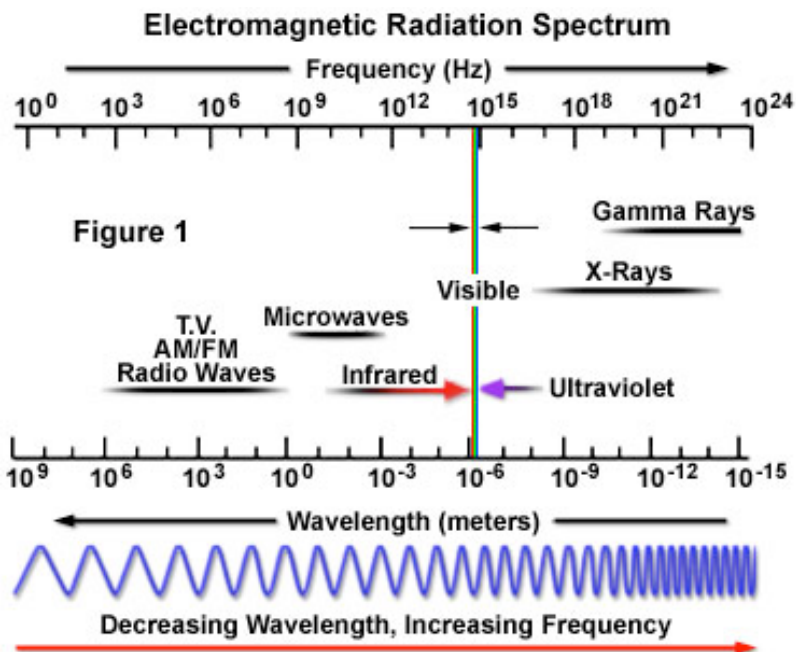

Halliday, Resnick, Walker Fundamentals of Physics, 1997

$$\mathbf{E}(z, t) = E_x \cos(kz - \omega t)\mathbf{e}_x + E_y \cos(kz - \omega t)\mathbf{e}_y$$

Figure 1

Cold neutrons (5×10^{-5}-0.025eV):
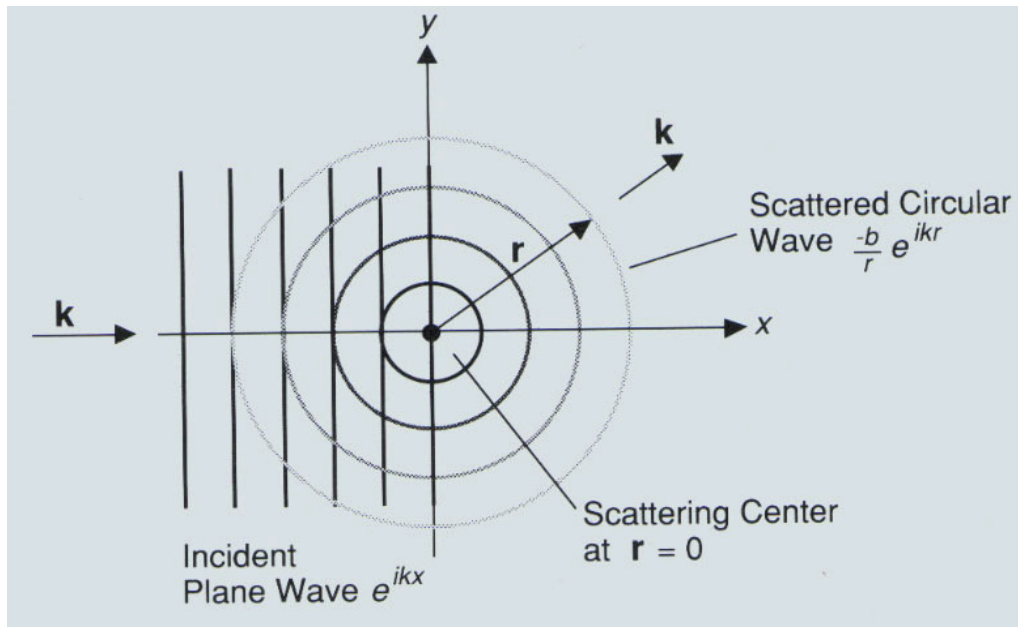
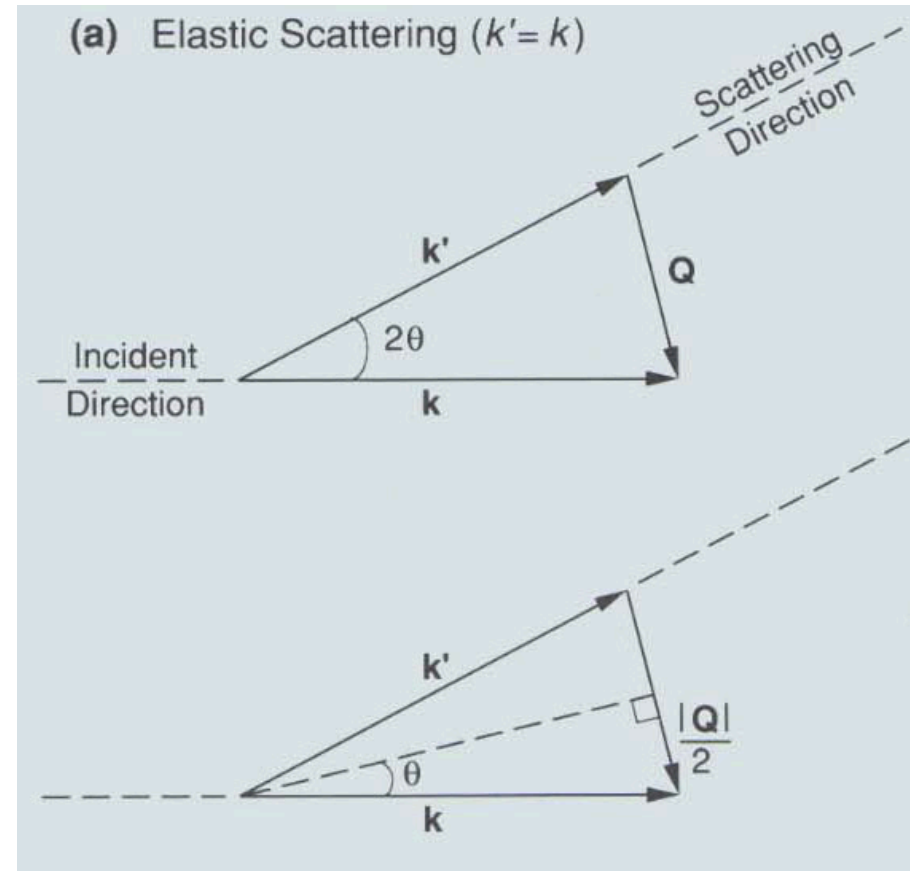$$\lambda_N = 0.2 - 2 \text{ nm}$$

$$\lambda = h/mv$$

Scattering basics

Scattering from single point

Scattered Circular Wave $\frac{-b}{r} e^{ikr}$

Scattering Center at $\mathbf{r} = 0$

Incident Plane Wave e^{ikx}

$$\sin \theta = \frac{q/2}{k}$$

$$q = 2k \sin \theta = \frac{4\pi \sin \theta}{\lambda}$$

Scattering vector

(a) Elastic Scattering ($k' = k$)

R. Pynn, Neturon Scattering–A primer, Los Alamos National Laboratory (1990).

Scattering from a lattice

Scattering intensity

$$I(\mathbf{q}) = \sum_{j,k} b^2 e^{i\mathbf{q}\cdot(\mathbf{r}_j - \mathbf{r}_k)}$$
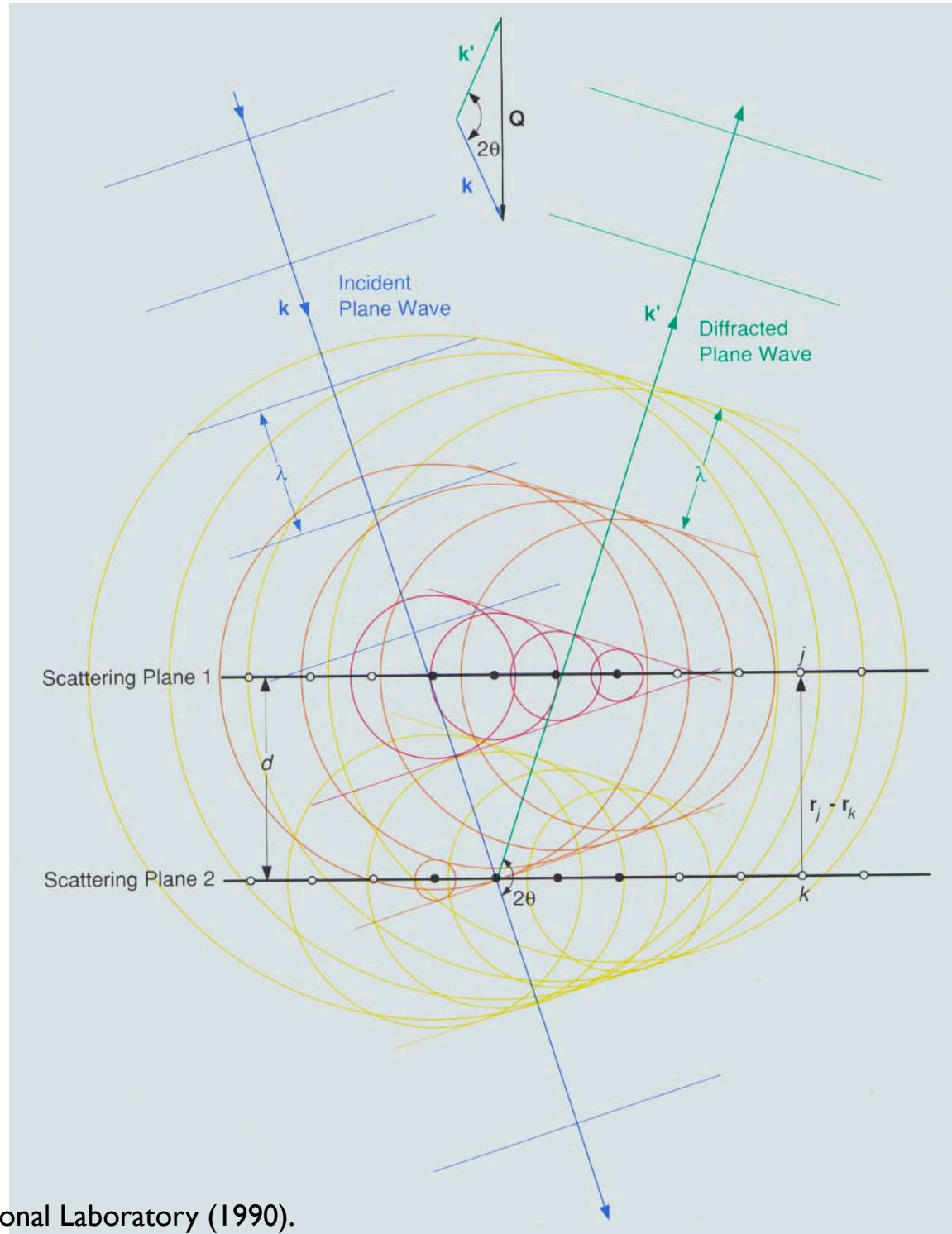
$$\equiv S(\mathbf{q})$$

Structure factor

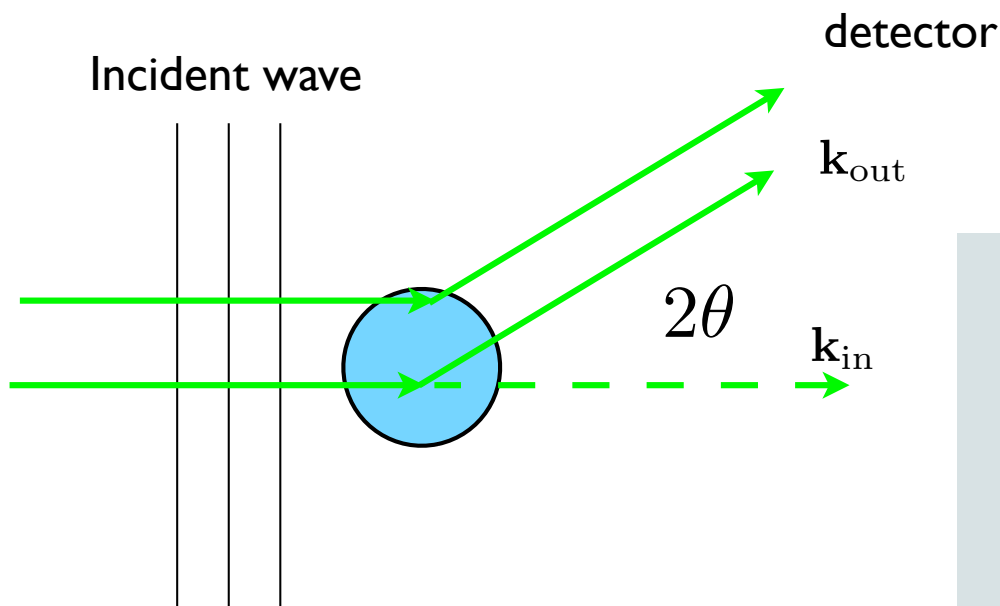$$\mathbf{q}\cdot(\mathbf{r}_j - \mathbf{r}_k) = qd = 2\pi n$$

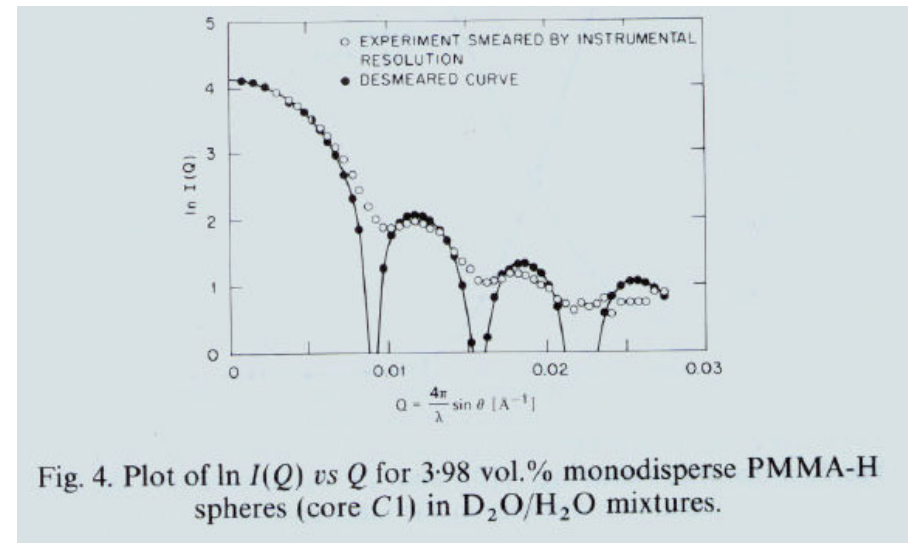$$q = (4\pi/\lambda)\sin\theta$$

Bragg's law: $n\lambda = 2d\sin\theta$

R. Pynn, Neturon Scattering–A primer, Los Alamos National Laboratory (1990).

Finite sized scatterer

Scattering from particle

$$P(q) = \left| \int_{V_p} d^3 r e^{i\mathbf{q}\cdot\mathbf{r}} \right|^2$$

Fig. 4. Plot of $\ln I(Q)$ vs Q for 3·98 vol.% monodisperse PMMA-H spheres (core C1) in D_2O/H_2O mixtures.

Total scattered intensity $I(q) \sim P(q)S(q)$

R. Pynn, Neturon Scattering–A primer, Los Alamos National Laboratory (1990).

Scattering from random media

Isotropic scatterers

Incident wave

detector

$\mathbf{k}_{out}$

$$I(\mathbf{q}) = \sum_{j,k} b^2 e^{i\mathbf{q}\cdot(\mathbf{r}_j - \mathbf{r}_k)} \equiv S(\mathbf{q})$$

2θ

$\mathbf{k}_{in}$

Structure factor relationship to RDF:

r_λ

$\mathbf{r}_k$

$\mathbf{r}_j$

$$S(q) = 1 + \frac{4\pi n}{q} \int_0^\infty r(g-1)\sin qr\, dr + \ldots$$
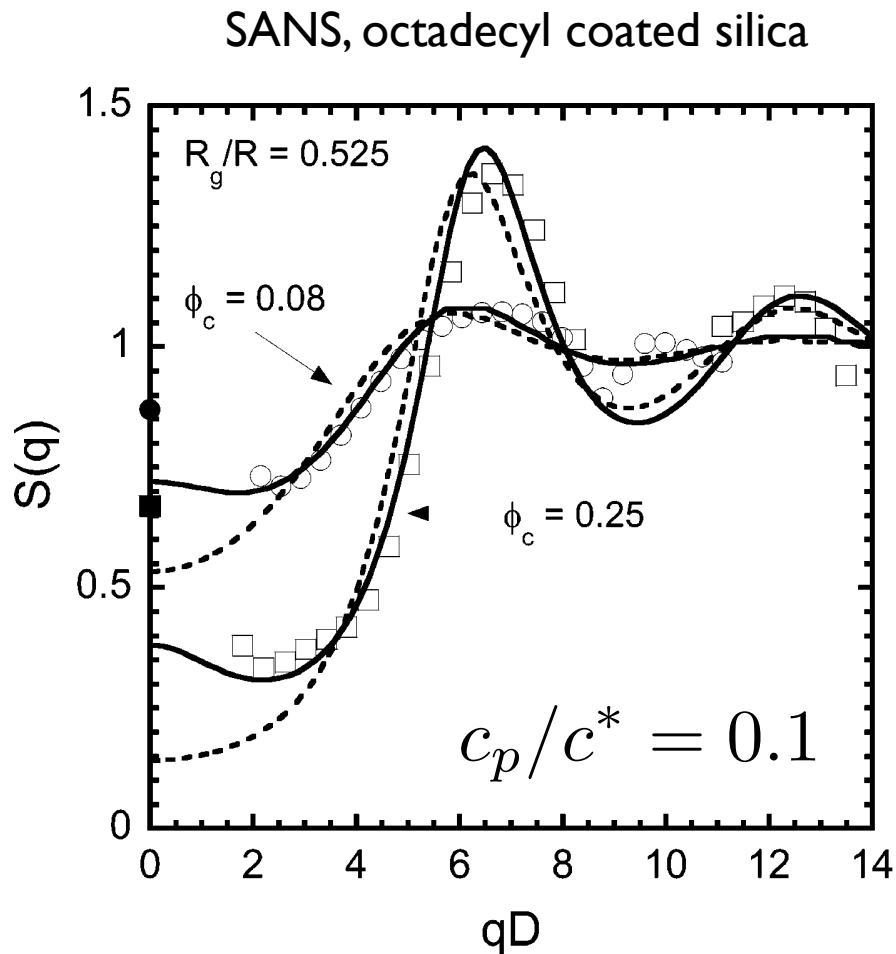
Radial distribution function

$$g(r_\lambda) = \frac{3\langle N_\lambda \rangle}{2\pi N \rho (r_{\lambda+1}^3 - r_\lambda^3)}$$

$\langle N_\lambda \rangle$ in $r_\lambda < r < r_{\lambda+1}$
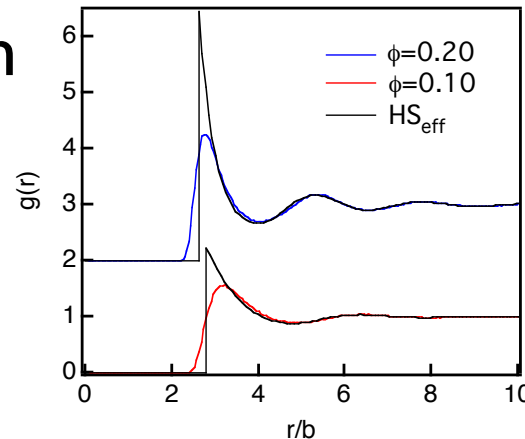
Measure of average "local" structure

J. Barker and D. Henderson, Ann. Rev. Phys. Chem. 23, 439 (1972).

Structure factor

SANS, octadecyl coated silica

Relationship to RDF

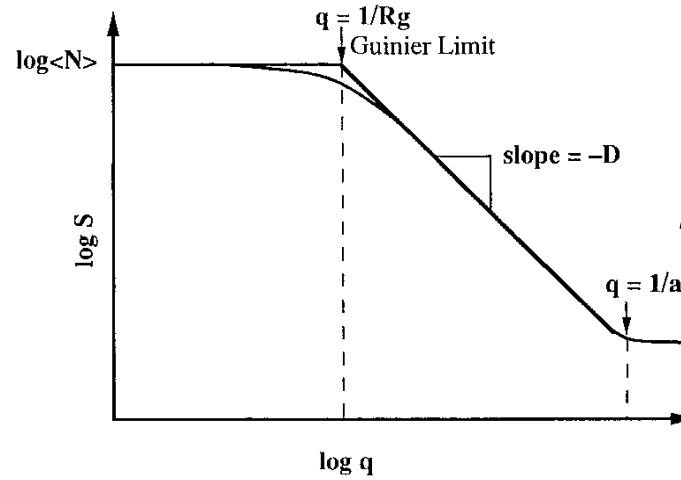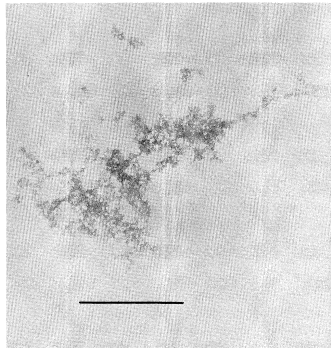$$S(q) = 1 + \frac{4\pi n}{q} \int_0^\infty r(g-1)\sin qr \, dr + \dots$$

Isothermal compressibility

$$S(0, \phi) = \frac{d\phi}{d[\phi Z(\phi)]}$$

$$Z(\phi) = \Pi / n k_B T$$

Π Osmotic pressure

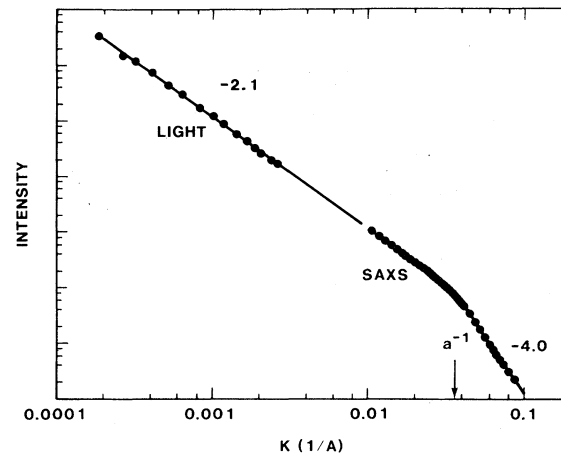S. A. Shah, et al., Langmuir 19, 5128 (2003).
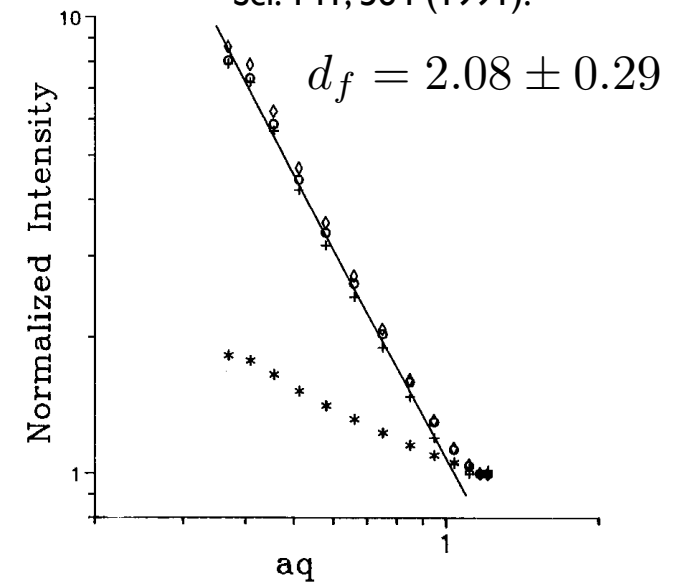
Fractal gels

$$S(q) \sim q^{-d_f}$$

Ludox silica in 0.5M NaCl

D. W. Schaefer, et al., Phys. Rev. Lett. 52, 2371 (1984).

Stoeber silica in hexadecane

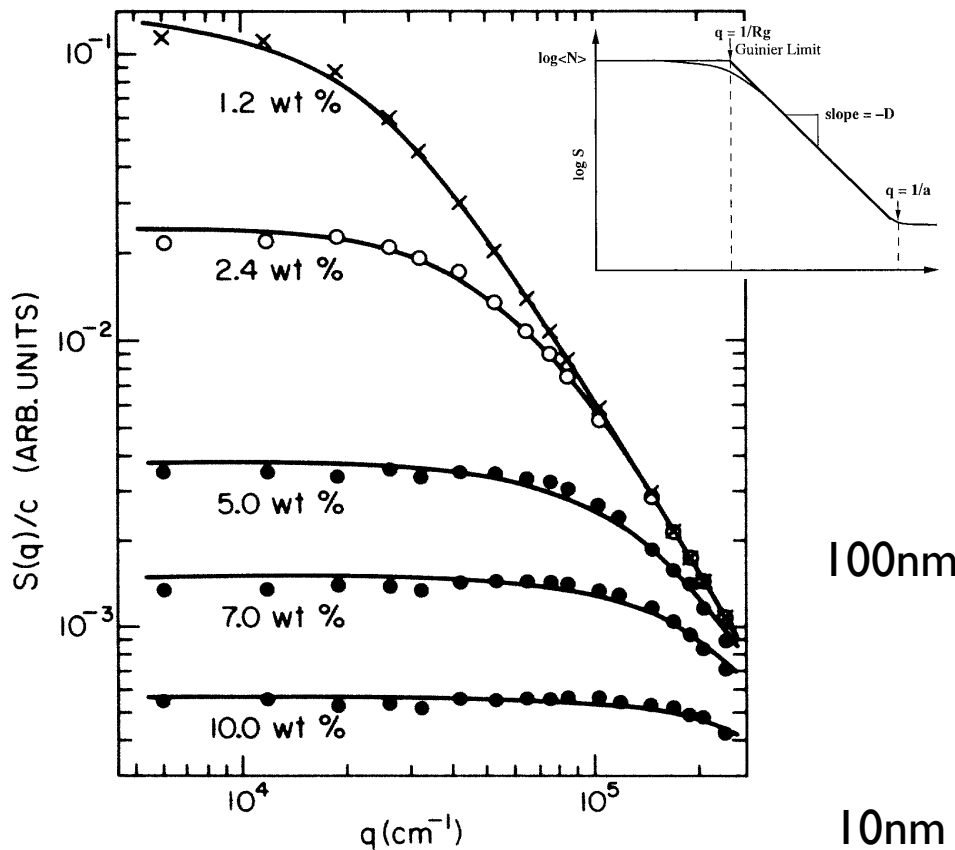M. Chen and W. Russel, J. Colloid Interface Sci. 141, 564 (1991).

$$d_f = 2.08 \pm 0.29$$

Fractal cut-off
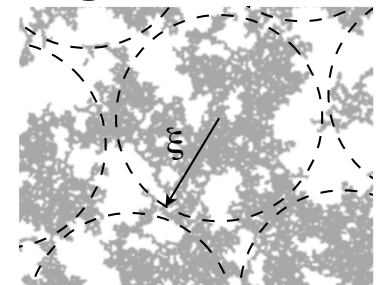
Model structure factor

Structure factor

7nm colloidal silica
0.45M NaCl, pH 7.0

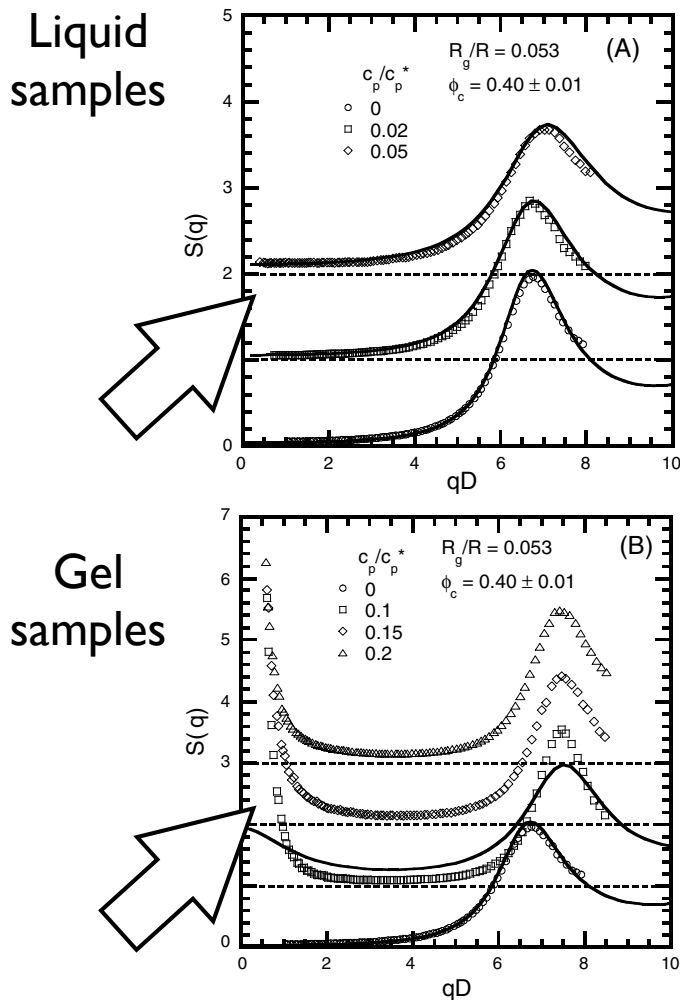$$S(q) = \frac{S(0)}{[1 + q^2\xi^2/(1+\alpha)]^{1+\alpha}}$$

$$\alpha = 0.08 \quad d_f \approx 2.16$$

"Cross-over length"

100nm

10nm

Low-q structure

S.A. Shah, et al., J. Phys.: Condens. Matter 15, 4751 (2003).
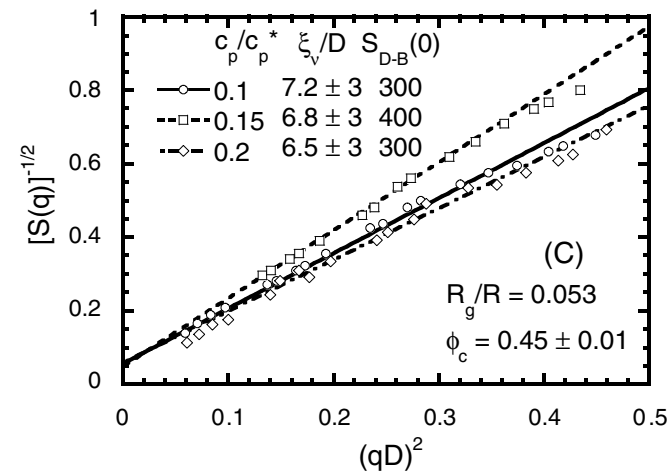
Liquid samples

Gel samples

Figure 3. Structure factor $S(q)$ as a function of the dimensionless wavevector qD for samples with varying amounts of polymer quantified by the dimensionless polymer concentration, c_p/c_p^*. The colloid volume fraction is fixed at $\phi_c = 0.40 \pm 0.01$ and $R_g/R = 0.053$. (A) Liquid samples: $c_p/c_p^* = 0$ (circles), 0.02 (squares) and 0.05 (diamonds). (B) Gel samples: $c_p/c_p^* = 0.1$ (squares), 0.15 (diamonds) and 0.20 (triangles), and as a reference $c_p/c_p^* = 0$ (circles). Each subsequent data set is offset by 1 for clarity. Dotted lines show relevant baselines signifying $S(q) = 0$ for each data set. Full curves are the zero-adjustable parameter PRISM-mPY theory predictions.

- **Low-q upturn: possibly void-like structures**

Debye-Bueche random two-phase model:

$$S_{\mathrm{DB}}(q) = \frac{S_{\mathrm{DB}}(0)}{(1 + q^2 \xi_\nu^2)^2}$$

$$S_{\mathrm{DB}}(0) = 48\phi \left(\frac{\xi_\nu}{D}\right)^3 \langle \eta^2 \rangle$$

Cluster precursors

V. Gopalakrishnan and C. F. Zukoski, Phys. Rev. E 75, 021406 (2007).

USAXS 42 nm silica, non-adsorbing polymer
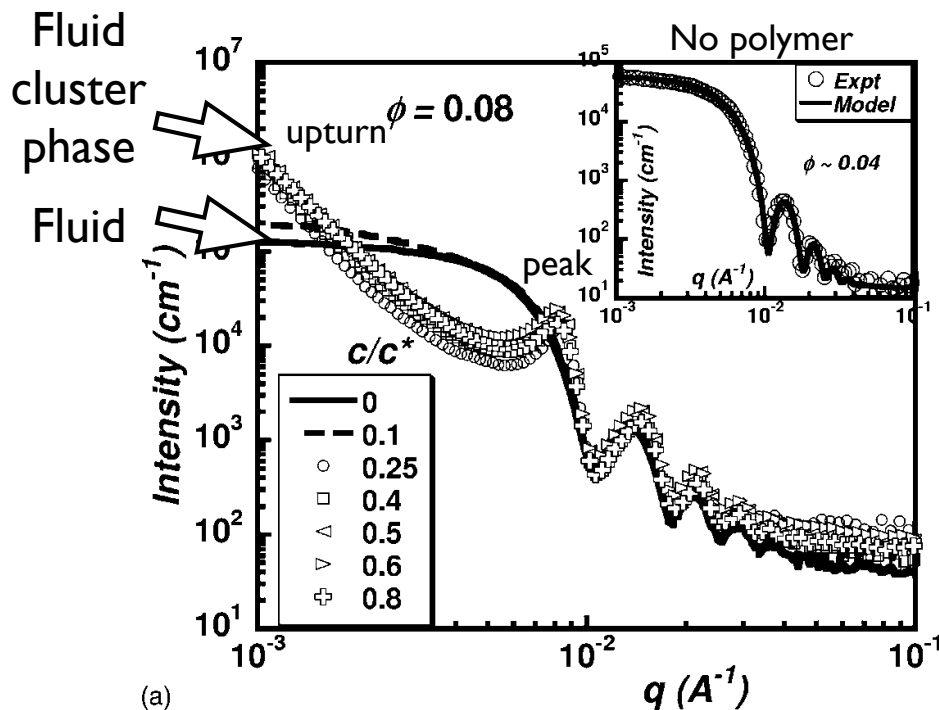
- Mobile cluster phase precursor to gel.

- Microstructure of the particle clusters are similar to that observed in dense space-spanning depletion gels.

- Percolation of the clusters due to settling does not influence their internal microstructure.

- Supports hypothesis that formation of space-spanning depletion gels is driven by the percolation of particle clusters.
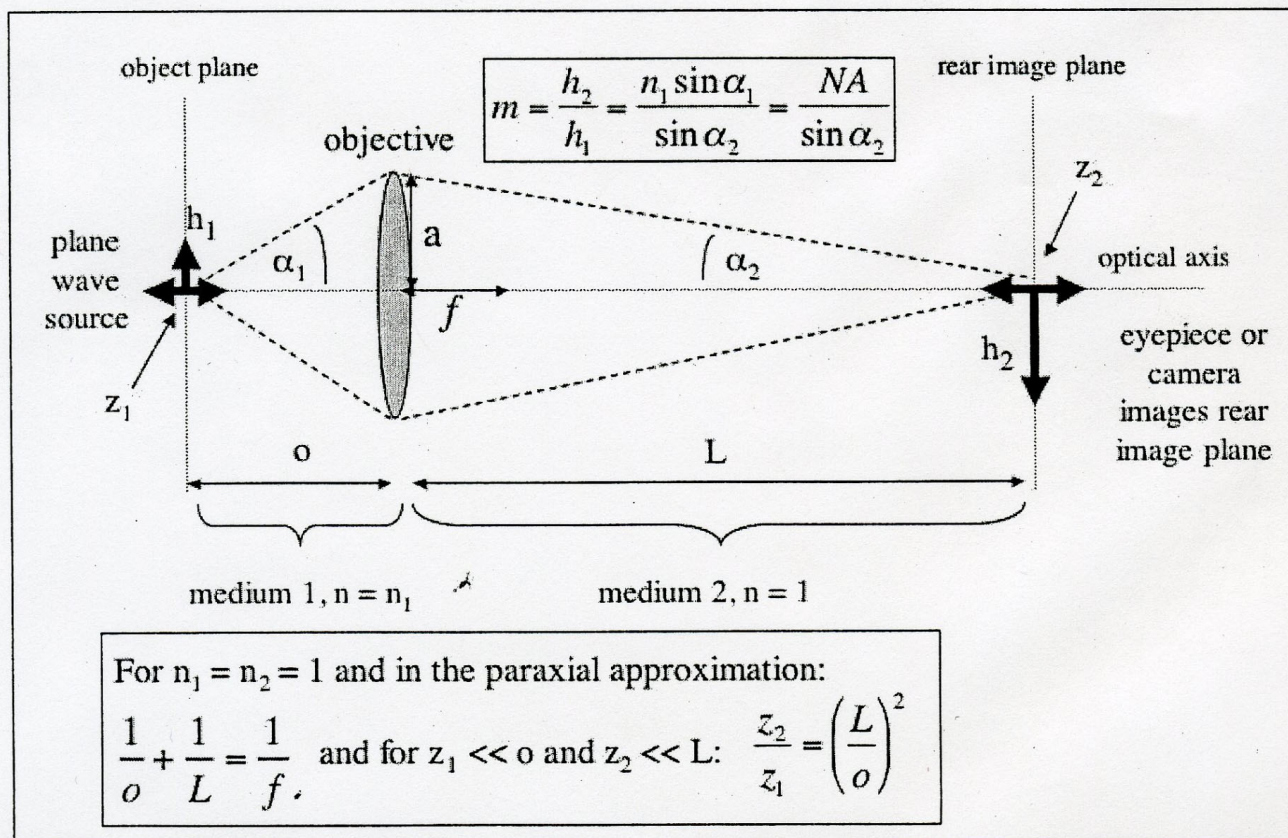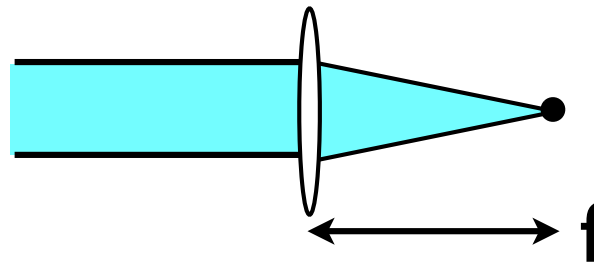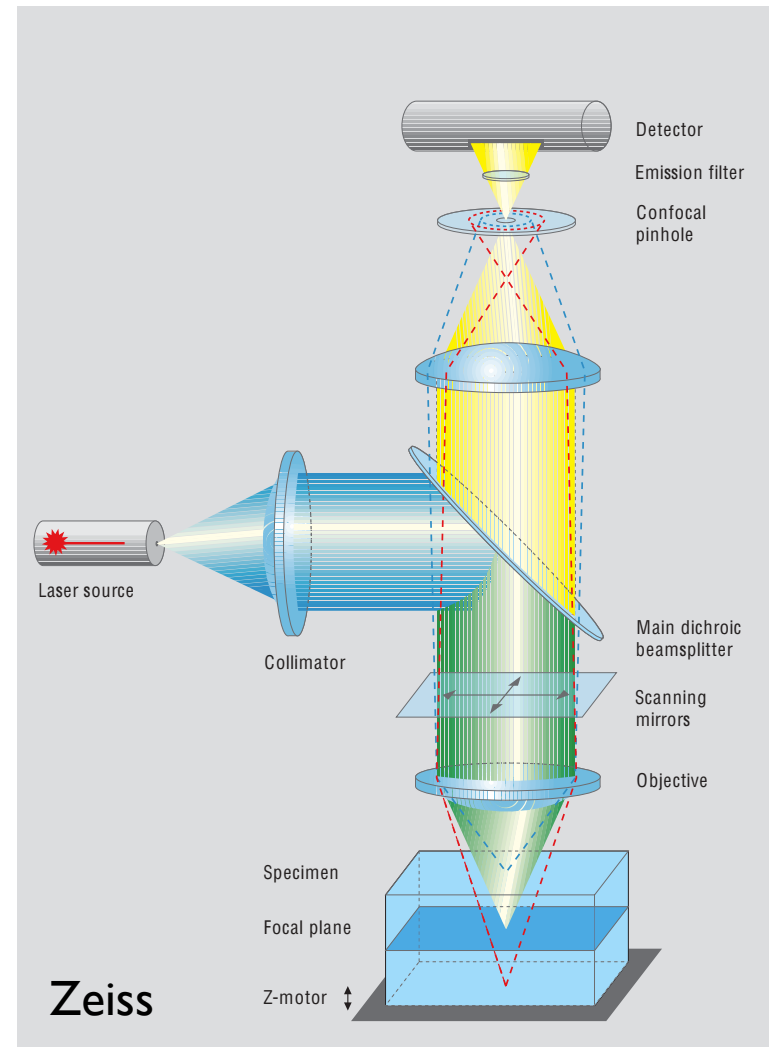
Microscopy

Basic imaging

Confocal imaging

- Prevents out-of-plane rays from contributing to image.

- Useful for imaging dense suspensions.

- Objective or stage is moved to collect multiple, vertically stacked images.

- Stacks are combined to create image volumes.

Zeiss

Confocal imaging in suspensions

- Requires specialized colloidal systems for index and density matching, i.e.

Fluorescent particle	Sterically-stabilized PMMA (a = 0.77 μm)
Index and density matched solvent	Decalin and cyclohexyl bromide
Non-adsorbing polymer	Polystyrene (M_w = 900,000), c*=5mg/ml
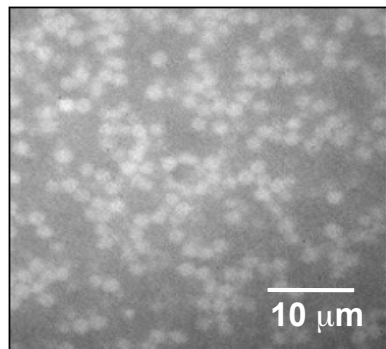
Fluorescent PMMA viewed
with confocal microscope

10 μm
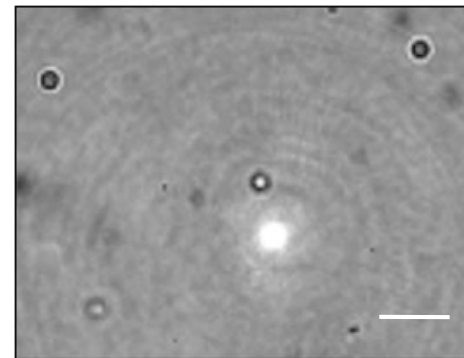
Dispersed melamine particles
viewed with bright-field
microscope in same suspension

Particle tracking

Crocker and Grier, J. Colloid Interface Sci., 179:298, 1996.

- Locate brightest pixel (x_0, y_0)

  - Calculate weighted centroid

$$\begin{pmatrix} \varepsilon_x \\ \varepsilon_y \end{pmatrix} = \frac{1}{m_0} \sum_{i^2 + j^2 \le w^2} \begin{pmatrix} i \\ j \end{pmatrix} \cdot A(x + i, y + j)$$
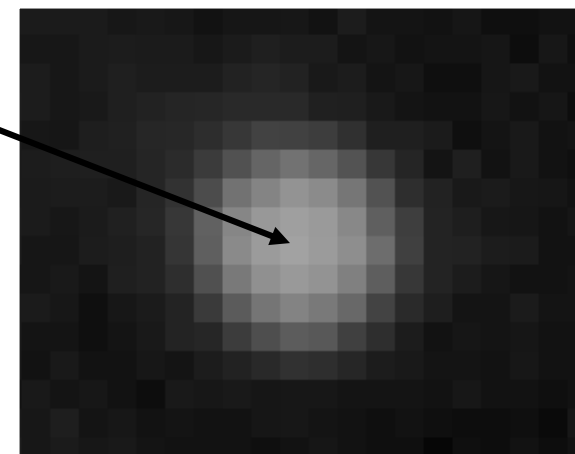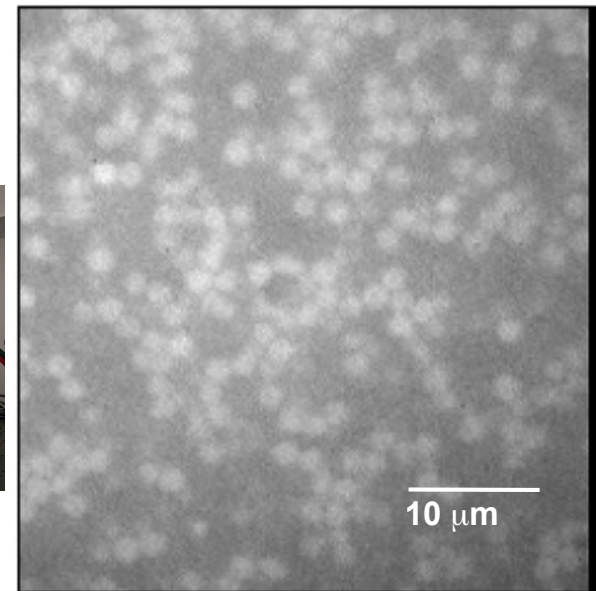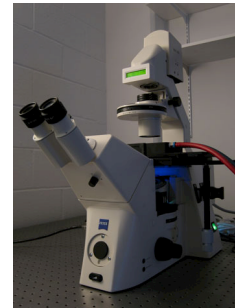
$$m_0 = \sum_{i^2 + j^2 \le w^2} A(x + i, y + j)$$

  - Refine location

$$(x, y) = (x_0 + \varepsilon_x, y_0 + \varepsilon_y)$$

- Resolution to fraction of pixel (~10 nanometers)

- Correct static and dynamic errors

- See http://www.physics.emory.edu/~weeks/idl/

- Static and dynamic error:

  T. Savin and P. S. Doyle, Biophys. J., 88:623–638, 2005.

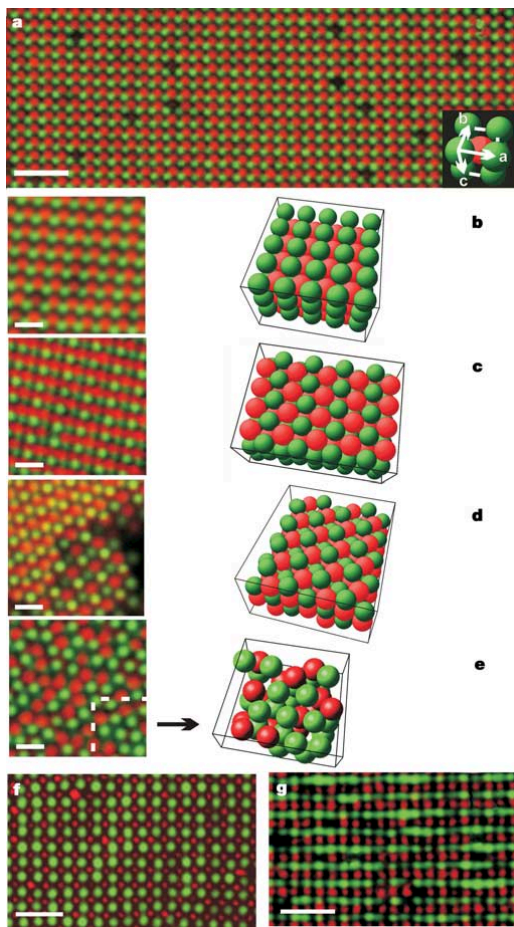(x_0, y_0)

10 μm

$w \longrightarrow$

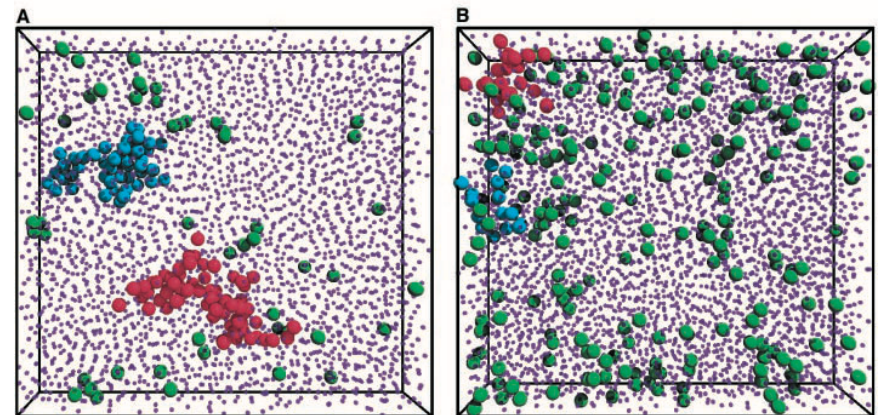# Information: all particle positions in a 3D volume

(Similar to simulations)
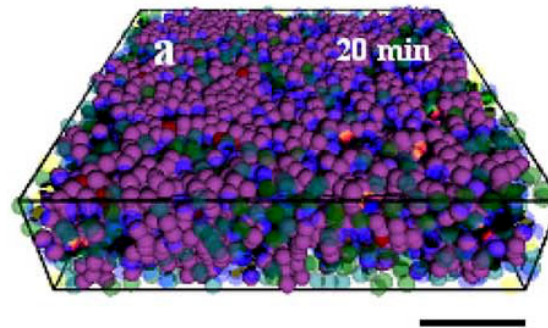

Colloidal crystals

M. E. Leunissen, et al., Nature 437, 236 (2005).

Glass dynamics

E. R. Weeks, et al., Science 287, 627 (2000).

Gels

Structure using microscopy

Radial distribution function
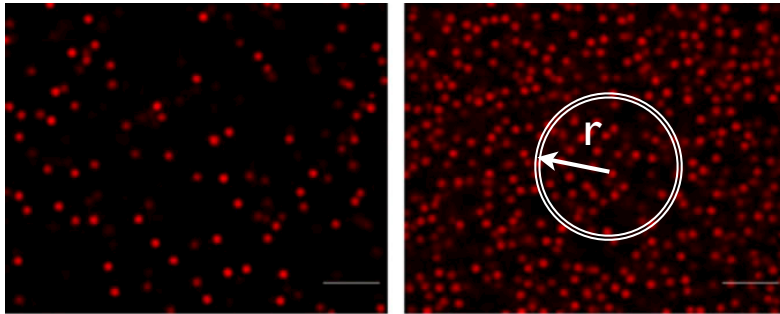
The radial distribution function is calculated directly from coordinates of particles.

$$g(r_\lambda) = \frac{3\langle N_\lambda \rangle}{2\pi N \rho (r_{\lambda+1}^3 - r_\lambda^3)}$$

$\langle N_\lambda \rangle$ in $r_\lambda < r < r_{\lambda+1}$

Images and data from M. Kogan, C. J. Dibble, R. E. Rogers, and M. J. Solomon, J. Coll. Int. Sci. 318, 252 (2007).

Integrated RDF

$$N(r) = 4\pi \int_0^r s^2 g(s) ds$$
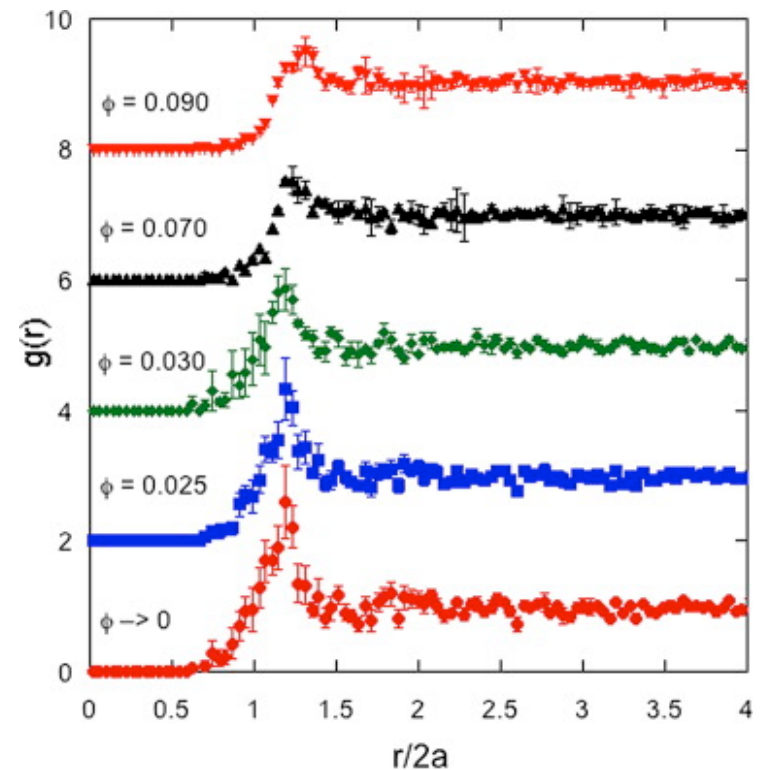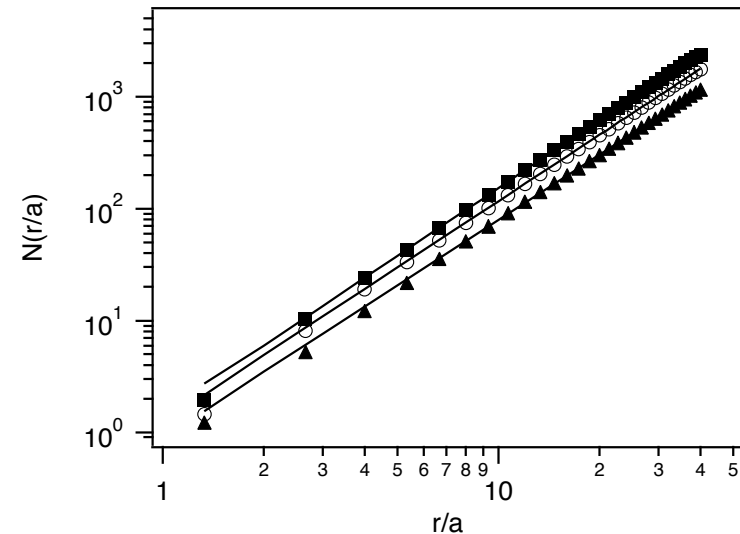
Randomly distributed fractal clusters

$$g(r) \sim Ar^{d_f - 3} \exp(-r/\xi)$$

Power-law scaling of integrated RDF

$$N(r) = N_0(\xi/a)^{d_f}$$

M. Hütter, J. Colloid Interface Sci. 231, 337 (2000).
F. Ferri, B. J. Frisken, and D. S. Cannell, Phys. Rev. Lett. 67, 3626, 1991.

Contact distribution

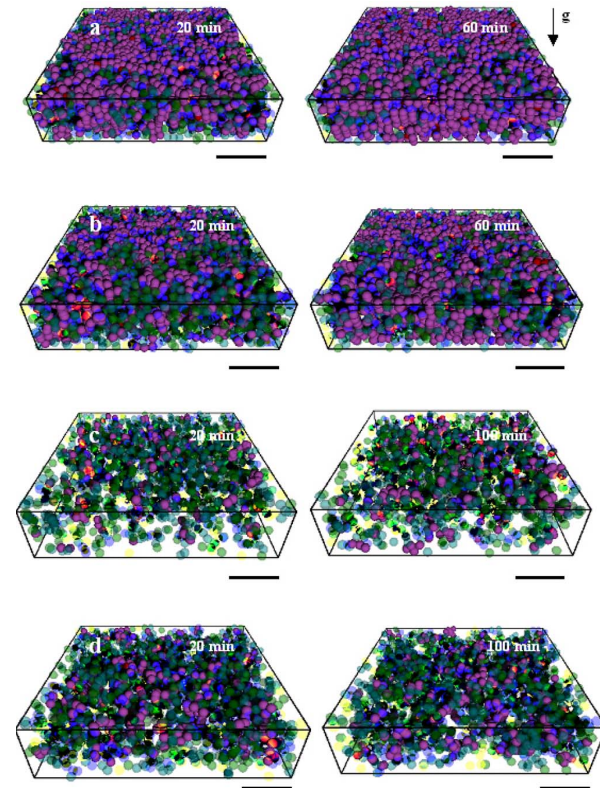## Local structure: average number of particles in "contact"

a.
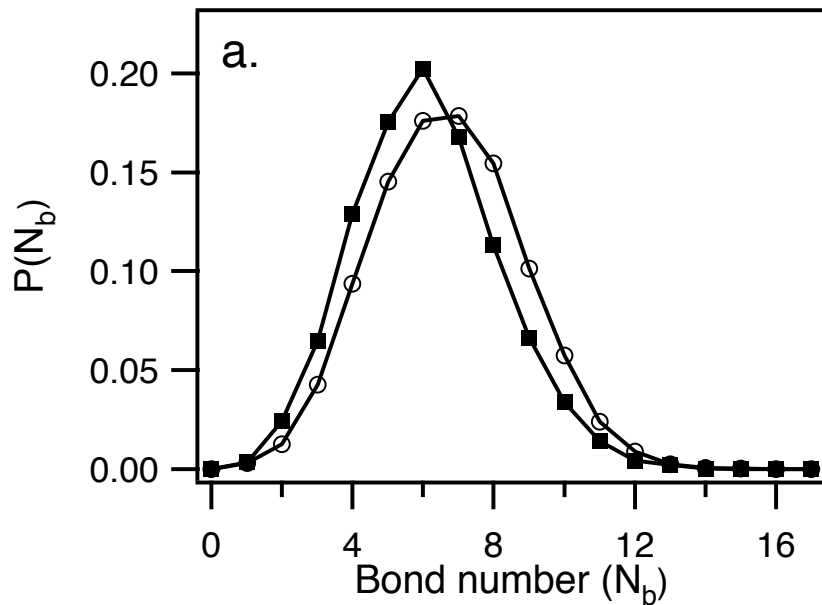
FIG. 9. Color online Visualizations of the structural evolution of sediments. a $C_P=0.0$ mg/ml; b $C_P=2.8$ mg/ml; c $C_P=4.1$ mg/ml; d $C_P=8.0$ mg/ml at $\phi_o=0.125$. Particles are described with seven different colors, depending the number of bonds per particles. A white circle means that a particle has no bond. Yellow, green, cyan, and blue represent one to four bonds, respectively. A pink indicates five to nine bonds. A red means greater than ten bonds. Particles with fewer than five bonds are rendered translucently.

Bond angle distribution

$$p(\theta + \delta\theta/2) = \frac{2\pi}{3} \frac{\delta N_\theta(\theta, \theta + \delta\theta)}{\delta\theta N_\theta^t}$$
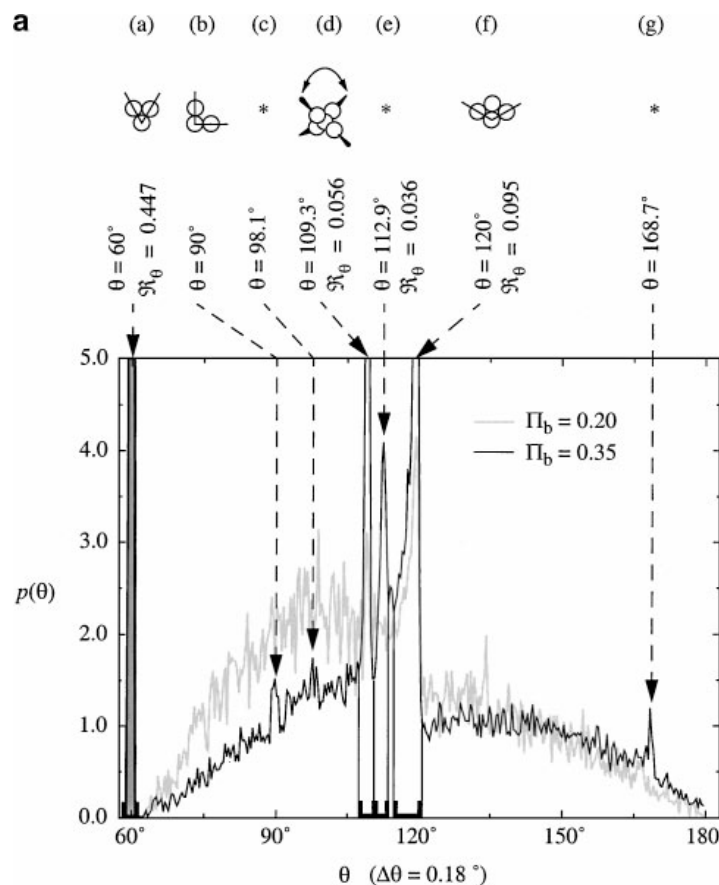
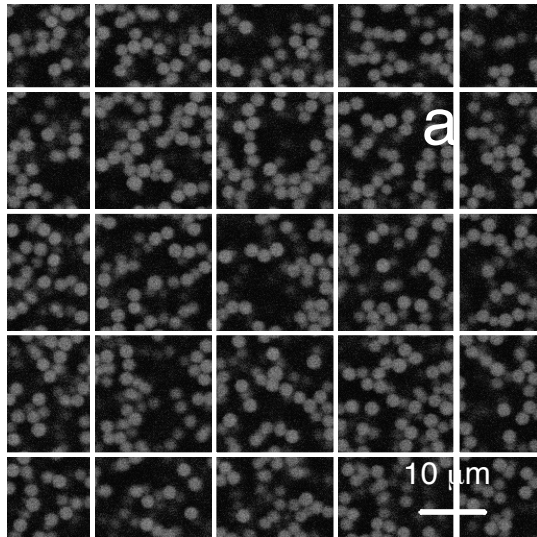$$\delta N_\theta(\theta, \theta + \delta\theta)$$

particle triplets
with bond angle
between

$$\theta, \theta + \delta\theta$$

$$N_\theta^t$$

Total number
particle triplets

M. Hütter, J. Colloid Interface Sci. 231, 337 (2000).

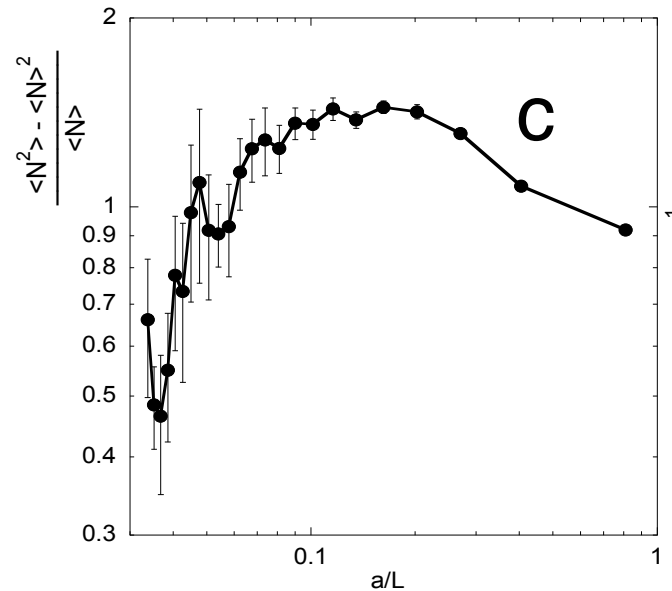# Density fluctuations
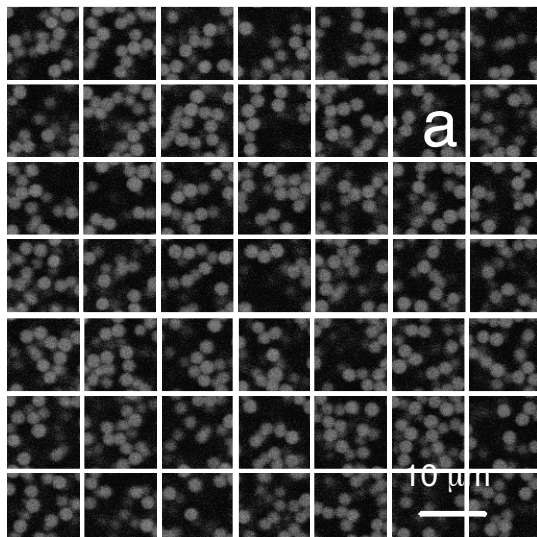
N Number of particles in volume L^3

$$\frac{\langle N^2 \rangle - \langle N \rangle^2}{\langle N \rangle^2}$$

Relationship to isothermal compressibility

$$\lim_{a/L \to 0} \frac{\langle N^2 \rangle - \langle N \rangle^2}{\langle N \rangle^2} = S(0) = \rho k_B T \chi_T$$

M. Kogan, C. J. Dibble, R. E. Rogers, and M. J. Solomon, J. Coll. Int. Sci. 318, 252 (2007).

Higher concentrations

FIG. 3. Representative 2D confocal micrographs of system structure as a function of increasing depletion pair potential strength. (a) $c/c^*=0.15$, (b) $c/c^*=0.21$, (c) $c/c^*=0.26$, (d) $c/c^*=0.31$, (e) $c/c^*=0.33$, (f) $c/c^*=0.37$, (g) $c/c^*=0.41$, (h) $c/c^*=0.46$, (i) $c/c^*=0.49$, (j) $c/c^*=0.64$, (k) $c/c^*=1.03$, (l) $c/c^*=1.54$.

- a-free particles
- b-mobile clusters coexist with free particles
- c-increasingly immobile clusters
- d,e,f,g-bicontinuous network
- h-maximum void structure
- i-more homogeneous, branched
- j,k,l-chain-like locally, homogeneous globally

Density fluctuations

C. J. Dibble, M. Kogan, and M. J. Solomon, Phys. Rev. E 74, 041403 (2006).

FIG. 6. Number density fluctuation measures show the normalized mean-squared fluctuations of particle number as a function of subsystem size considered as it varies with attraction strength for a $c/c^* \leq 0.46$ and b $c/c^* \geq 0.49$. c Mean number-density fluctuations for all attraction strengths for inverse length scale $a/L=0.101$.

Contact number distribution

C. J. Dibble, M. Kogan, and M. J. Solomon, Phys. Rev. E 74, 041403 (2006).

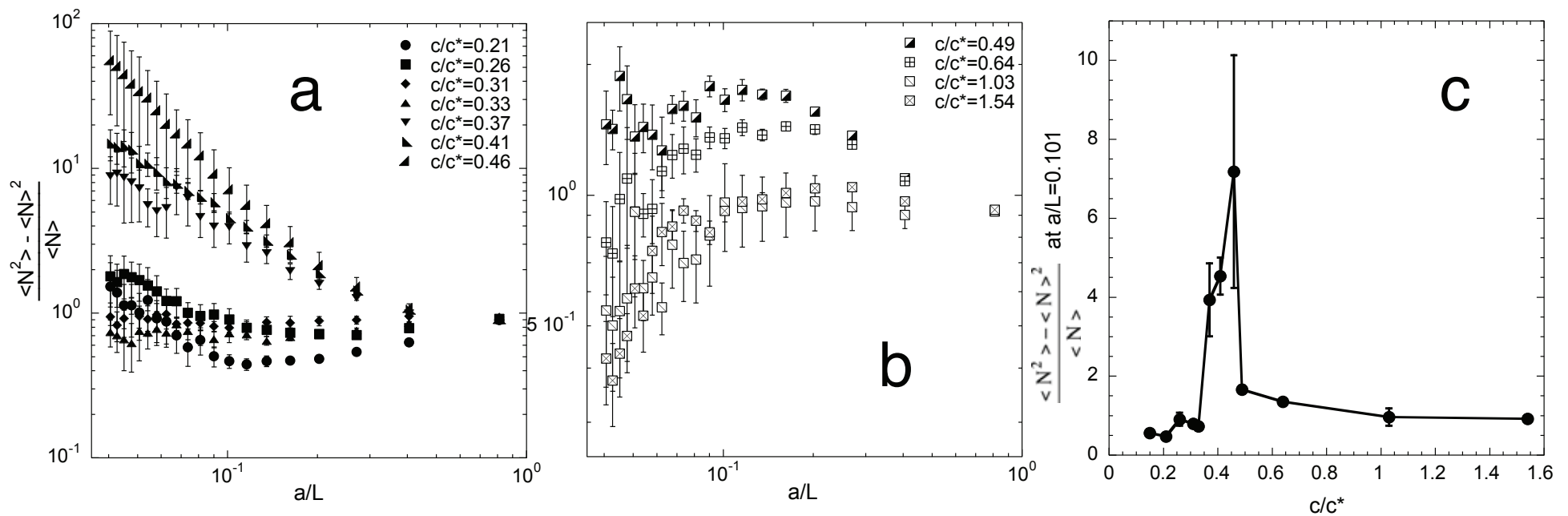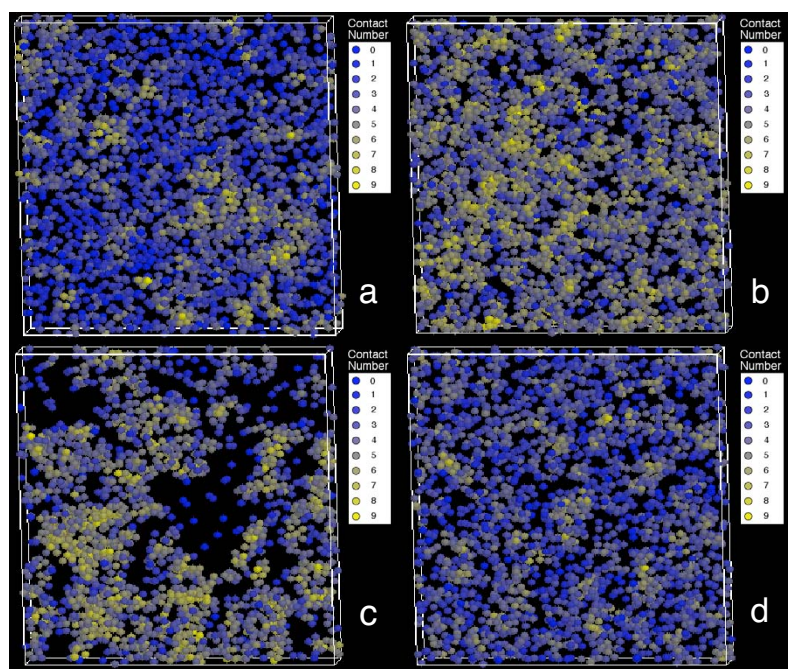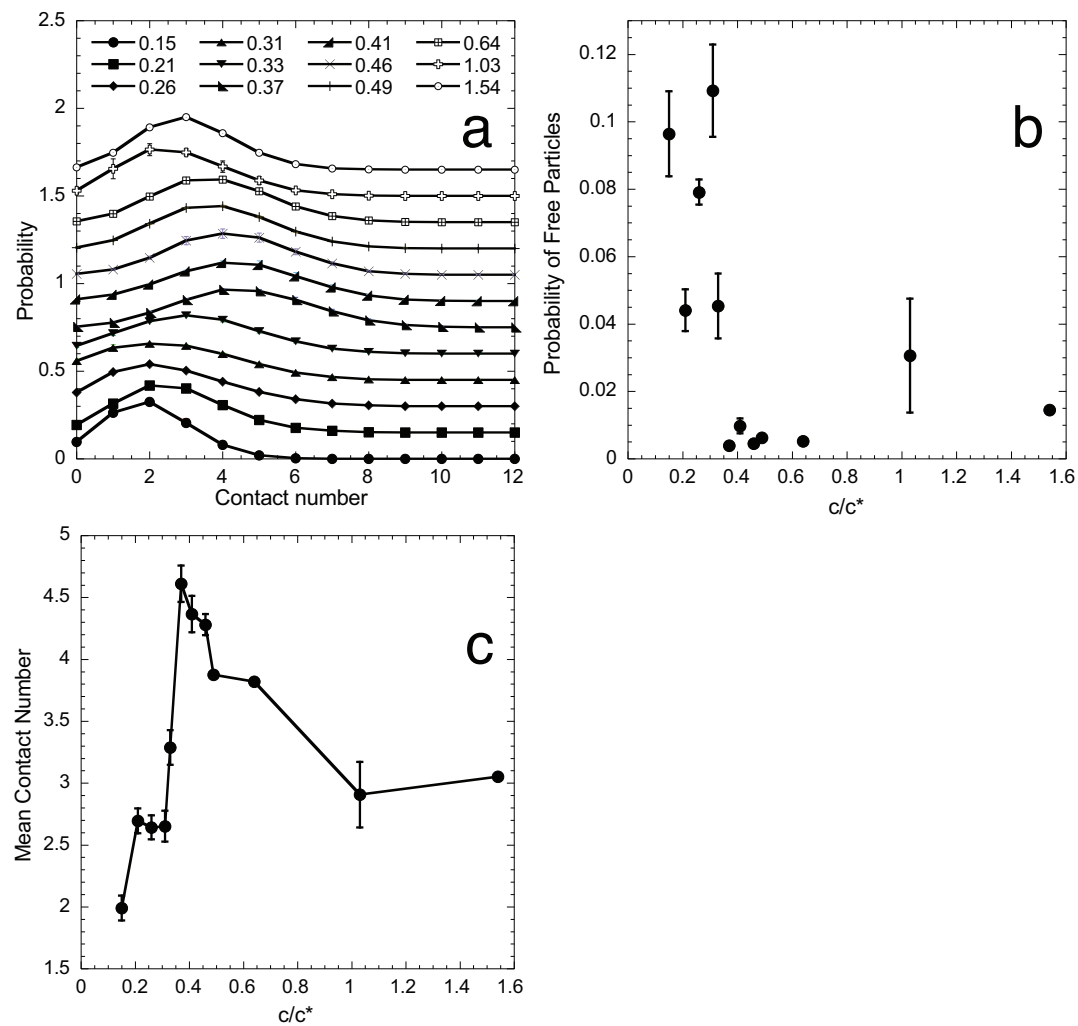FIG. 4. (Color online) Shaded representation depicts spatial dependence of contact number on depletant concentration for (a) $c/c^* = 0.26$, (b) $c/c^* = 0.37$, (c) $c/c^* = 0.41$, (d) $c/c^* = 1.03$ where lighter shading (yellow color online) correspond to high contact numbers and darker shading (blue color online) correspond to low contact numbers.
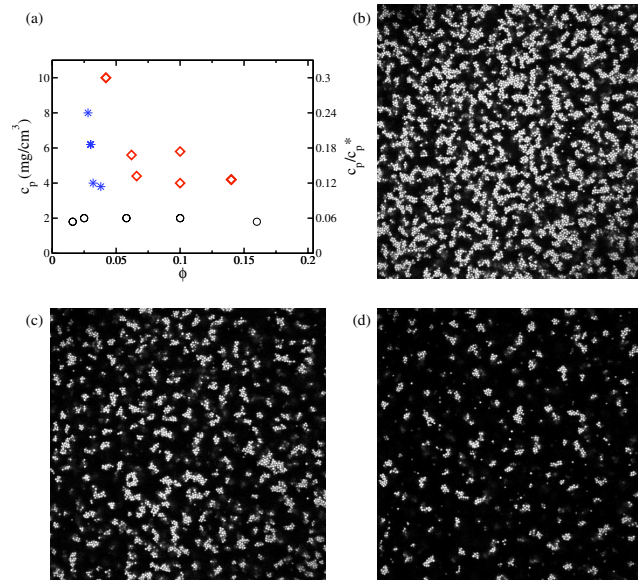
"Route to gelation is highly dependent on the state of density matching and charge of the constituent particles"

H. Sedwick, S. U. Egelhaaf, and W. C. K. Poon, J. Phys: Condens. Matter 16, S4913 (2004).

Screened, density-matched
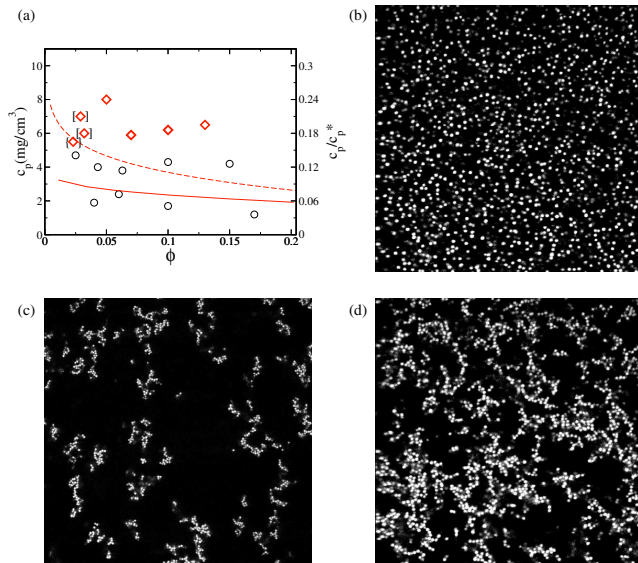
Screened, density-mismatched

Charged, density-matched
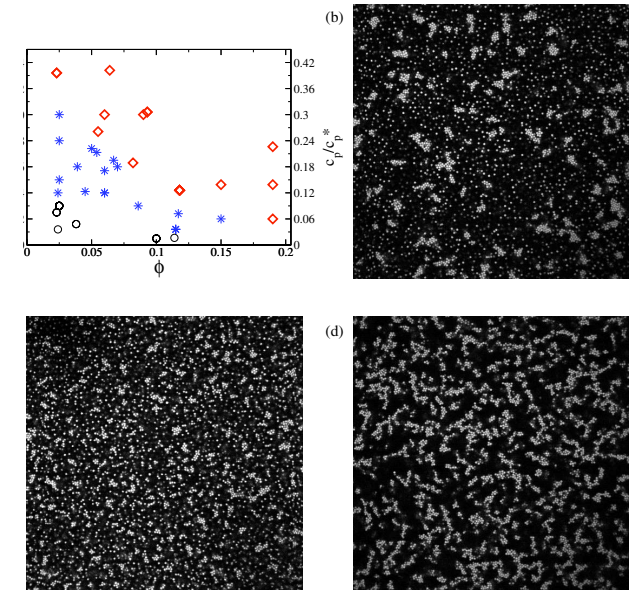
Figure 3. (a) Observations of the charged, density-matched system ($Q\bar{G}$) of $\delta \approx 0.021$. Symbols represent the following: fluid—circle, mobile clusters—star, and frozen structures—diamond. (b) A confocal micrograph of the clusters in a sample with $\phi = 0.086$ and $c_p = 3$ mg cm^{-3}. (c) A confocal micrograph of the clusters in a sample with higher volume fraction, $\phi = 0.15$, and $c_p = 1.9$ mg cm^{-3}. (d) A confocal micrograph of the frozen structure at $\phi = 0.083$ and $c_p = 6$ mg cm^{-3}.

Long-range repulsion

A. I. Campbell, V. J. Anderson, J. S. van Duijvenveldt, and P. Bartlett,
Phys. Rev. Lett. 94, 208301 (2005).

Transition from cluster phase to gel

Unusual local order in network:
face-sharing tetrahedral clusters
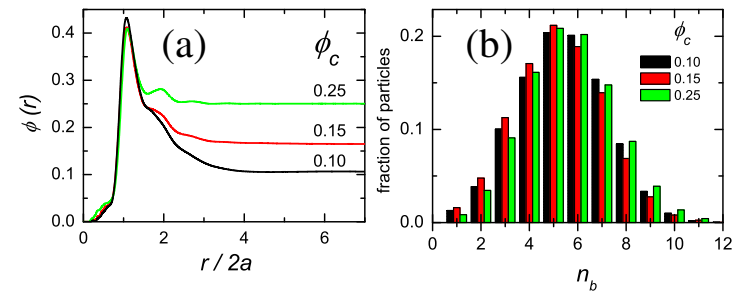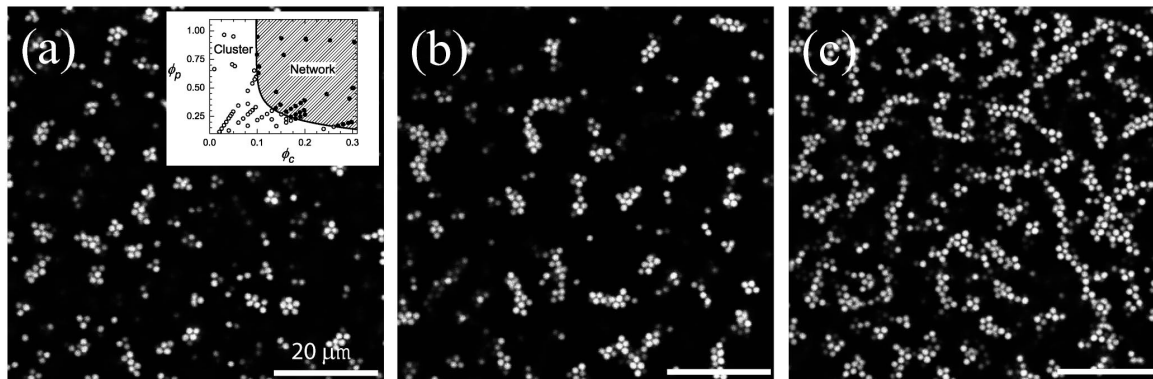
- Long-range repulsive interactions alters dynamical arrest.
- Formation of stable, chain-like clusters, constructed from face-sharing tetrahedral units, which associate into a fully connected network at gelation.
- Does formation of tetrahedra reflect the presence of charge or is simply a consequence of a centrosymmetric attractive potential?

Dynamic scattering

Light scattering

$\mathbf{k}_i$

θ

$\mathbf{k}_s$

$\mathbf{q}$

$I(\mathbf{q}, t)$

$$E(t) = \sum_{i=1}^{N} E_i \exp\left[i\mathbf{q} \cdot \mathbf{r}_i\right]$$

$\Delta\Phi$

speckle pattern

sample
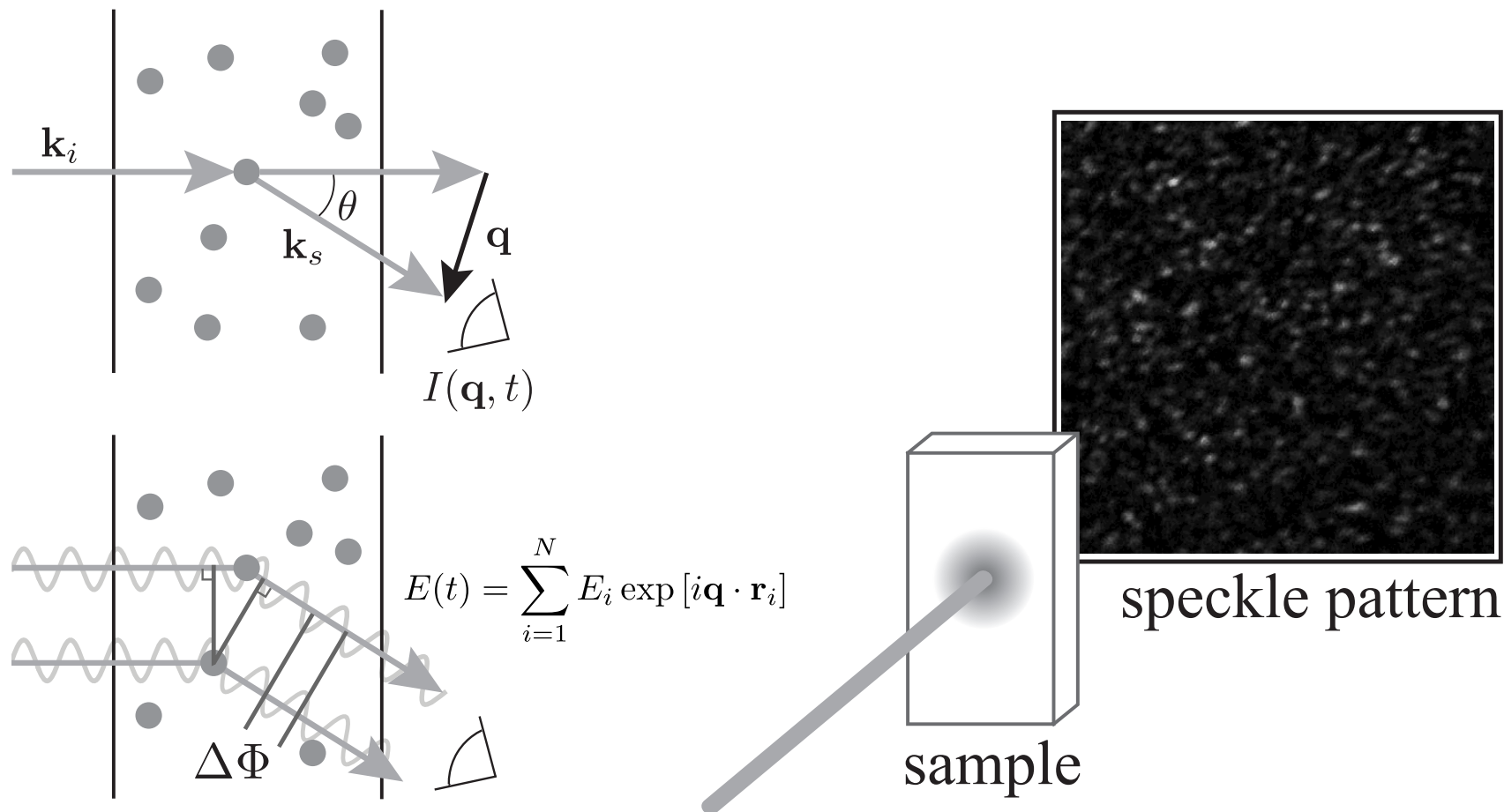
$$q = |\mathbf{q}| = (4\pi n/\lambda_v)\sin\theta/2 \quad \textit{scattering vector}$$

Intensity fluctuations

$\mathbf{k}_i$

θ

$\mathbf{k}_s$

$\mathbf{q}$

$I(\mathbf{q}, t)$

$\Delta\Phi$

speckle pattern

sample

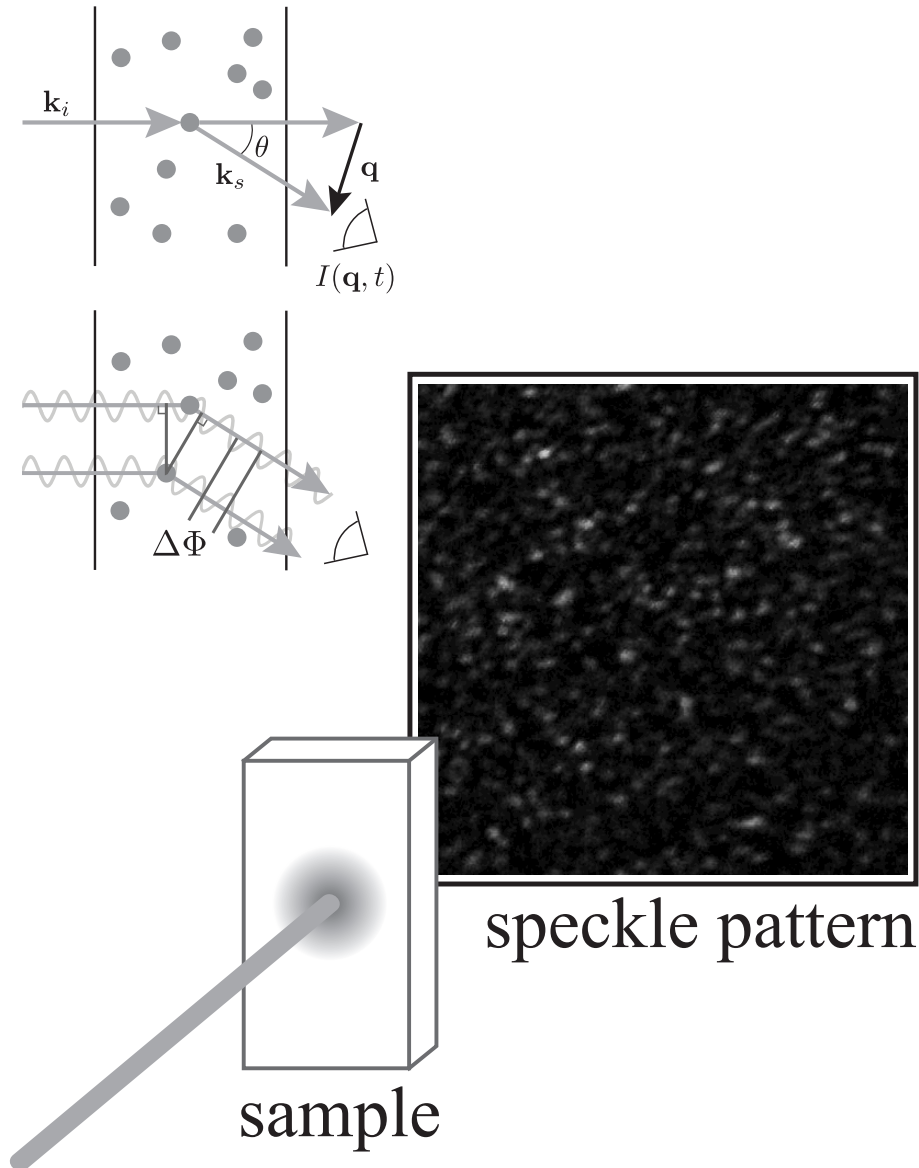### Intensity fluctuations

$I(t_0)$ $I(t_0 + t)$

$\langle I \rangle$

$\sqcup t$ lag time

time

Intensity correlation function

2

$g^{(2)}(t)$

$\dfrac{\langle I(t_0)I(t - t_0)\rangle}{\langle I \rangle^2}$

$\dfrac{\langle I^2 \rangle}{\langle I \rangle^2}$

$\dfrac{\langle I \rangle^2}{\langle I \rangle^2}$

1

0

10^{-5} 10^{-4} 10^{-3} 10^{-2} 10^{-1}

$t\,(\mathrm{s})$
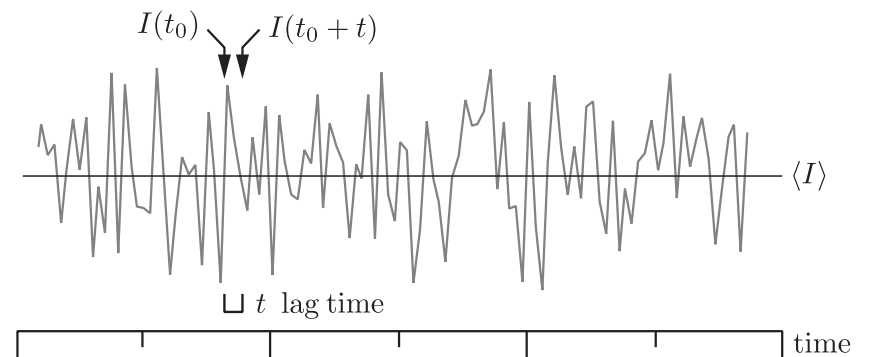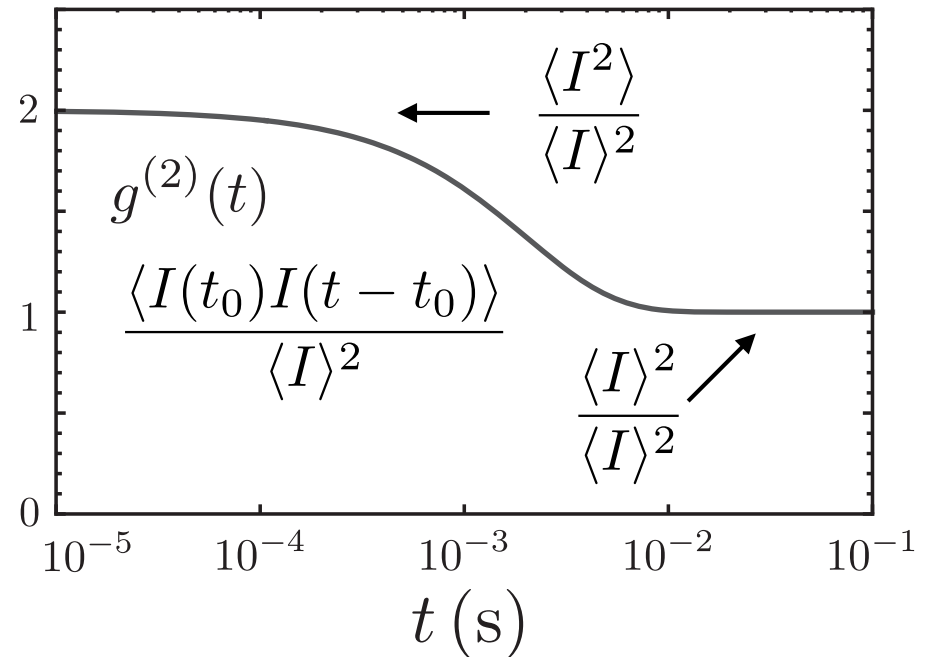
Light scattering microrheology

Intensity correlation function

$$g^{(2)}(t)$$

$$\frac{\langle I(t_0)I(t-t_0)\rangle}{\langle I\rangle^2}$$

$t\,(\mathrm{s})$
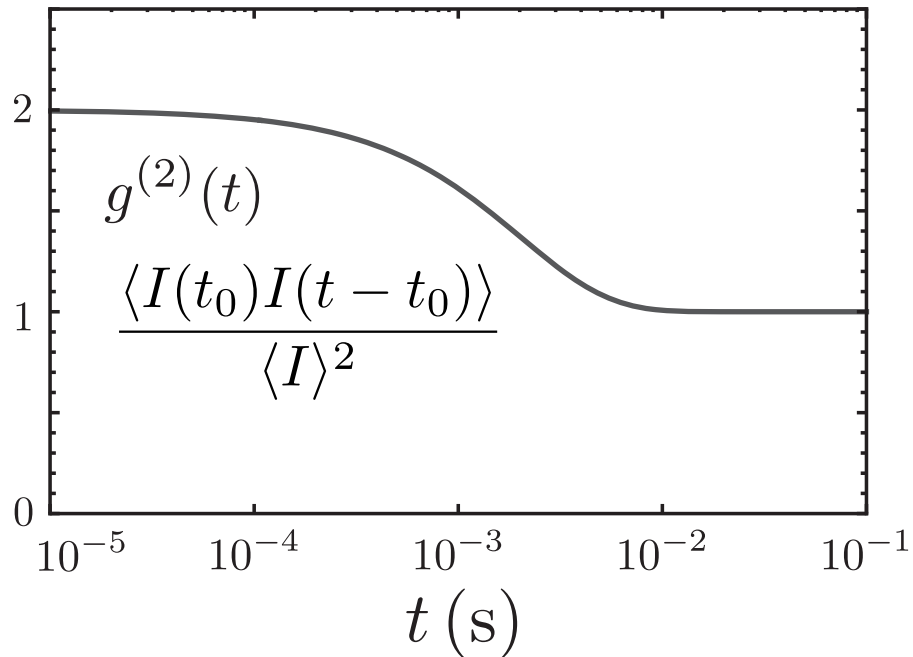
Field correlation function

$$g^{(1)}(t) = \frac{\langle E(t)E^*(0)\rangle}{\langle |E(t)|^2\rangle}$$

$$g^{(1)}(t) = \exp\left[\frac{-q^2\langle\Delta r^2(t)\rangle}{6}\right]$$

Siegert relation

$$g^{(2)}(t) = 1 + \beta|g^{(1)}(t)|^2$$

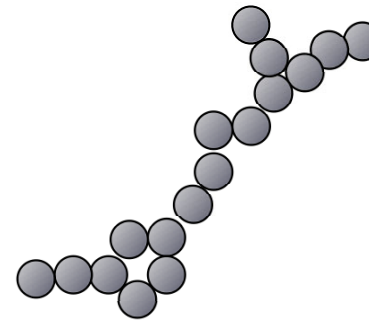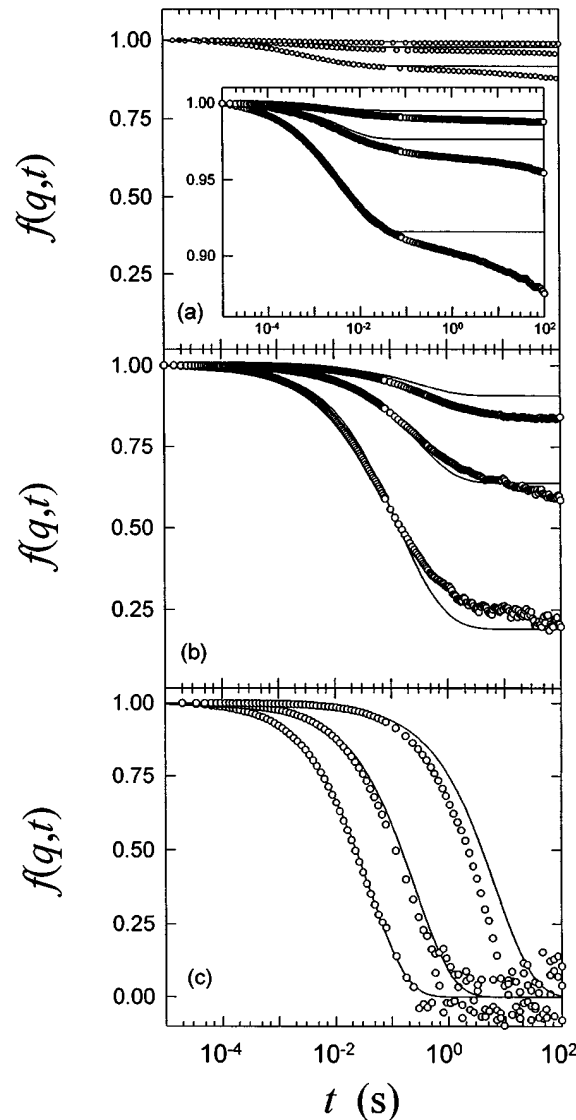# Internal dynamics and elasticity of fractal colloidal gels

Krall, A. H. & Weitz, D. A. *Phys. Rev. Lett.* **80**, 778–781 (1998).

$$\tau(s) = 6\pi\eta s/\kappa(s)$$

$$\tau(s) = \tau_0(s/a)^{\beta+1}$$

$$\langle \Delta r_\xi^2(t) \rangle_s = \frac{2k_BT}{n(s)\kappa(s)}\{1 - e^{-t/\tau(s)}\}.$$

$$n(s) = N_c(a/s)^{d_f}$$

number of regions size s

segment rigidity

$$\kappa(s) = \kappa_0(a/s)^\beta$$

$$\beta = 2 + d_B$$

Integrate over density of modes $dn(s)/ds$

$$\langle \Delta r_\xi^2(t) \rangle = 2d_f k_BT \int_\xi^{R_c} \frac{ds}{s\kappa(s)}\{1 - e^{-t/\tau(s)}\}.$$

$$\xi = q^{-1}$$

FIG. 1. Dynamic structure factors $f(q,t)$ of fractal colloidal gels for different ϕ_0 and q; (a) $\phi_0 = 5.0 \times 10^{-3}$, and $q = 4.1$, 8.7, and 16.7 μm^{-1} from top to bottom; smooth curves are theoretical fits yielding $\delta^2 = 1.9 \times 10^{-3}$ μm^2 and $\tau = 3.9 \times 10^{-3}$ s; (b) $\phi_0 = 1.5 \times 10^{-3}$; $q = 4.1$, 8.7, and 16.7 μm^{-1}; $\delta^2 = 3.5 \times 10^{-2}$ μm^2, $\tau = 0.36$ s; and (c) $\phi_0 = 1.7 \times 10^{-4}$; $q = 4.1$, 12.1, and 22.3 μm^{-1}; $\delta^2 = 13$ μm^2, $\tau = 1850$ s.

Methods summary

Technique	Advantages	Disadvantages
Neutron	• Works for many materials • Bulk samples (1-2mm) • Rheo-SANS	• Ensemble averaged structure • Accessibility
X-ray	• Works for many materials	• Ensemble averaged structure • Shorter penetration lengths • Accessibility
Light	• Convenience • Simultaneous rheology	• Ensemble averaged • Specialized experimental systems (index match)
Confocal	• Direct, real space structure • Simultaneous dynamics	• Specialized experimental systems (index, density match) • Flow studies limited by frame rate
Electron	• Detailed particle size, shape information	• Sample preparation • Vacuum technique